Heterogeneous Crystallization of the Phase Change Material GeTe via Atomistic Simulations

Gabriele C. Sosso,[*,†,‡] *Matteo Salvalaglio,*[†,‡,¶] *Jörg Behler,*[§] *Marco Bernasconi,*[‖] *and Michele Parrinello*[†,‡]

Department of Chemistry and Applied Biosciences, ETH Zurich, Vladimir-Prelog-Weg 1-5 CH-8093 Zurich, Switzerland, Faculty of Informatics, Università della Svizzera Italiana, Via G. Buffi 13, CH-6900 Lugano, Switzerland, Institute of Process Engineering, ETH Zurich, Sonneggstrasse 3, CH-8092 Zurich, Switzerland, Lehrstuhl für Theoretische Chemie, Ruhr-Universität Bochum, Universitätsstrasse 150, D-44780 Bochum, Germany, and Dipartimento di Scienza dei Materiali, Università di Milano-Bicocca, Via R. Cozzi 55, I-20125 Milano, Italy

E-mail: gabriele.sosso@phys.chem.ethz.ch

[*]To whom correspondence should be addressed
[†]ETH Zurich
[‡]Università della Svizzera Italiana
[¶]ETH Zurich
[§]Ruhr-Universität Bochum
[‖]Università di Milano-Bicocca

Abstract

Phase change materials are the active compounds in optical disks and in non-volatile phase change memory devices. These applications rest on the fast and reversible switching between the amorphous and the crystalline phases, which takes place in the nano domain in both the time and the length scales. The fast crystallization is a key feature for the applications of phase change materials. In this work, we have investigated by means of large scale molecular dynamics simulations the crystal growth of the prototypical phase change compound GeTe at the interface between the crystalline and the supercooled liquid reached in the device upon heating the amorphous phase. A Neural Network interatomic potential, markedly faster with respect to first principles methods, allowed us to consider high-symmetry crystalline surfaces as well as polycrystalline models which are very close to the actual geometry of the memory devices. We have found that the crystal growth from the interface is dominant at high temperatures while it is competing with homogeneous crystallization in the melt at lower temperatures. The crystal growth velocity markedly depends on the crystallographic plane exposed at the interface, the (100) surface being kinetically dominant with respect to the (111) surface. Polycrystalline interfaces, representative of realistic conditions in phase change memory devices, grow with at significantly slower pace due to presence of grain boundaries.

Keywords: Crystal Growth, Phase Change Materials, Supercooled Liquids, Molecular Dynamics.

Introduction

The relentless increase in the power of consumer, computer and communication electronics requires data storage technologies able to keep up with the pace of data production and exchange. Several options are under scrutiny for new non-volatile memory devices suitable to overcome the limitations in speed and downscale of the current FLASH memories. Among these, phase change memories (PCM) based on chalcogenide alloys are particularly promising.[1–4] Indeed, 45 nm feature-size PCMs have already been delivered for mobile applications, and memory cells below the 20 nm length scale have been developed as well.[4,5] Materials in the same class are also used in optical data storage (DVD and Blue rays)[1] and, more recently, in the realization of components for neuromorphic computing.[6,7] These applications rest on the ability of chalcogenide alloys to undergo upon heating a very fast (on the ns time scale[8]) and reversible transformation between the crystalline and amorphous phases, which display a large contrast in electrical and optical conductivity.[1,2,9] However, the timescale of the phase transition makes a direct experimental characterization of crystallization kinetics at the operation conditions very challenging.[10–12] On the other hand, the same very short transformation timescale stimulated the study of the early stage of the crystallization process by molecular dynamics (MD) simulations based on density functional theory (DFT).[13–15] Still, to extract quantitative information on the nucleation rate and crystal growth velocity and provide an effective comparison with experiments, large length and time scales are required, far beyond the reach of DFT simulations. As a route to overcome the limitations of DFT-MD methods we have developed interatomic potentials based on the fitting of a large DFT database by means of a Neural Network (NN) scheme.[16–18] We have recently used this scheme to generate a NN potential for the compound GeTe,[19] a prototypical phase change material that shares many properties with $Ge_2Sb_2Te_5$ (GST),[20–23] the alloy actually used in PCMs. The NN potential allows simulating tens of thousand of atoms for tens of ns by retaining an accuracy close to that of the underlying DFT potential energy surface. Using this potential we have tackled a comprehensive investigation of GeTe,[20,24] including

a quantitative estimate of the activation energy for the homogeneous crystallization in the supercooled liquid.[25] We have demonstrated that the high speed of homogeneous crystallization is actually due to the high diffusivity at low temperatures, which in turn boosts both the nucleation rate and the growth velocity of supercritical nuclei. The large self-diffusion coefficient at low temperatures is a manifestation of the fragility of the supercooled liquid, which shows a breakdown of the Stokes-Einstein relation due to the emergence of dynamical heterogeneities in the liquid .[25,26]

However, at operating conditions the crystallization process of GeTe does not proceed via homogeneous nucleation. Instead, the growth progresses from the interface between the polycrystalline material and the amorphous region.[27–29] In this work, we have thus undertaken this last step towards an atomistic modeling of the crystallization process in PCM by studying the propagation of the crystalline front at the interface between crystalline and supercooled liquid GeTe by means of very large (10^4 atoms) NN-MD simulations. In fact, when crystallization in PCM devices takes place, the amorphous phase is brought to a temperature much higher than the glass transition temperature T_g. The phase transformation typically occurs from a supercooled liquid phase[4] just below the melting temperature T_m (exp. 998 K[30]). On the other hand, T_g is believed to be close to the crystallization temperature detected by differential scanning calorimetry (T_x=400-450 K[34]). Thus, we shall refer throughout the paper to such temperature range when discussing explicitly T_g, although the heat capacity step associated with the glass transition has not been clearly reported for GeTe nor for several other phase change materials. We have thus studied the crystallization process at the representative temperatures of 500 K and 700 K during the quenching of the supercooled liquid in contact with the crystal. To this end we have used slab models to describe the interface between the crystal and the supercooled liquid. We have performed simulations for the two most relevant crystal faces of the cubic rock salt phase of GeTe, namely the (100) and (111) surfaces, as well as for a representative model of a polycrystalline surface which is very close to the real configuration experimentally realized in PCM

devices.

In the following we will demonstrate that homogeneous nucleation in the melt and crystalline growth at the liquid-crystal interface are competing processes close to the glass transition temperature. It turns out that the crystal growth at the interface is diffusion limited in the whole temperature range considered (500-700 K), and that it proceeds following a continuous growth mechanism which leads to a finite surface roughness. We have also found that the crystal growth velocity depends on the crystallographic planes at the crystal-liquid interface. In fact, the (111) surface grows slower than the (100), as in time it develops small three-sided pyramids exposing {100} facets. We observe the same trend in the case of the polycrystalline interface as well, where different grains tend to grow by faceting along {100} planes. The fact that the (100) surface is kinetically dominant in this temperature range might concur to the formation of the octahedral shape of GeTe micro-crystals exposing the slowest growing {111} planes that have been observed experimentally.[31,32]

Results and Discussion

(100) surface

Starting from an initially ideal crystalline slab in contact with the melt the system is equilibrated at fixed temperature. This procedure leads to a solid-liquid interface with a finite roughness. Details of the protocol employed to generate and equilibrate all the interface models are reported in the Supporting Information (SI). The crystalline part of the slab was prepared in the cubic rock-salt phase of GeTe (β phase) which is stable at high temperature and transforms into the trigonal ferroelectric (α) phase[33] at a critical temperature reported in the range 623-705 K.[34,35] As it is unclear whether this critical temperature can be accurately reproduced by the DFT functional underlying our NN potential, we have used the cubic lattice of the rock salt structure also at the lower temperature of 500 K. The local trigonal distortion with the alternation of short and long bonds of α-GeTe can actually arise,

albeit distributed in a random manner, also by using a cubic supercell.[36] To assess possible finite size effects, we have studied two different interface models (M1 and M2) with different aspect ratio of the in-plane and vertical sizes as given in Tab. 1. The calculated speed of crystal growth (cf. Tab. 1) turns out to be the same for the two models indicating that the smaller one is already unaffected by finite size effects. Thus, we refer in this section to M1 only, while results for the M2 model are reported for comparison in the SI (Fig. S1). We label an atom as crystalline or not according to the value of the order parameter $\bar{Q}_4$ described in the SI.

Table 1: Details of the models of the interface between supercooled liquid and crystalline GeTe (see text). N_{at} is total number of atoms in the model, N_{bulk} is the number of crystalline layers before crystallization takes place, hkl are the Miller indexes of the crystalline plane in contact with the liquid, and u is the crystal growth velocity. The crystal growth front proceeds along the c axis. In the case of the polycrystalline model MP, N_{bulk} cannot be defined (nd=undefined). M111$_T$ refers to the trigonal crystalline phase.

Model	N_{at}	Cell vectors [Å]			N_{bulk}	hkl	u [m/s]	
		a	b	c			500 K	700 K
M1	10240	48.59	48.59	127.91	8	100	1.7 ± 0.2	9.3 ± 0.4
M2	24576	97.18	97.18	76.07	8	100	1.7 ± 0.2	9.3 ± 0.4
M111	11600	76.85	73.95	60.32	7	111	0.9 ± 0.2	8.2 ± 0.4
M111$_T$	9084	50.12	49.61	111.25	7	111	0.7 ± 0.2	0.0000
MP	32768	99.27	99.27	99.27	nd	mix	0.7 ± 0.6	6.8 ± 0.5

The kinetics of crystal growth is different at the two temperatures considered of 500 K and 700 K. At 700 K the probability of nucleation from the melt is very low, and thus the crystal grows from the interface until the crystalline phase has filled the whole of the simulation box, leading to the formation of a single crystal. On the other hand at 500 K, the nucleation probability is much higher, such that a significant number of crystalline clusters nucleates in the melt and grows simultaneously with the growth of the crystalline front from the interface.

We have monitored the number of crystalline nuclei as a function of time at both 500 K and 700 K (panel a) of Fig. 1). Snapshots of the growing surface at both temperatures

are shown in panel b) of Fig. 1. The presence of crystalline nuclei in the melt hinders the crystalline growth from the interface. This is shown in panel c) of Fig. 1, reporting the time evolution of the effective thickness of the crystalline slab L_{cr}, which is defined by

$$L_{cr} = N_{cr} \cdot \frac{d_{hkl}}{2N_{surf}} \tag{1}$$

where N_{cr} is the number of crystalline atoms at time t, d_{hkl} is the spacing between (hkl) crystallographic planes, and N_{surf} is the number of atoms in a pristine crystalline surface layer. The factor $1/2$ accounts for the fact that two crystal fronts are growing simultaneously from the two sides of the crystalline slab. The d_{100} spacing is ~ 3.04 Å and depends very little on temperature. The speed of crystal growth u_{hkl} is then obtained from the slope of L_{cr} as a function of time.

While at 700 K the growth is linear in time until the two crystalline surfaces merge, at 500 K the linear regime holds only in the very early stages of crystallization. Once the crystalline surface starts to interact with the nuclei inside the melt, the speed of crystal growth decreases, as the nuclei have different orientations with respect to the growing (100) surface. Ordering atoms at grain boundaries is in fact a process slower than crystal growth from the interface. Therefore, in spite of the simultaneous crystal growth from the interface and from homogeneous nucleation, the increase in the number of crystalline atoms in the whole sample slows down with time at 500 K as shown in Fig. S2 of SI.

The speed of crystal growth obtained from the linear growth regime of the (100) surface is comparable, although slightly higher, to what we have previously obtained from simulations of the homogeneous crystallization.[25] We must consider that the small growing nuclei in the melt simulated previously exposed different crystallographic planes and that, as we shall see in the next sections, the crystallographic orientation plays a significant role in the crystal growth kinetics. Note that the temperature dependence of the speed of crystal growth u obtained here can be well described by the expression derived from classical nucleation theory for diffusion-limited crystallization[37,38]

$$u(T) = \frac{6D(T)}{\lambda}(1 - e^{-\frac{\Delta\mu(T)}{k_B T}}) \quad (2)$$

where D is the self diffusion coefficient, λ a typical jump distance for diffusion, and $\Delta\mu$ is the free energy difference between the crystal and the supercooled liquid at temperature T. Indeed, by substituting in the above expression the values for the self-diffusion coefficient computed by NN simulations in Ref.,[24] those for $\Delta\mu$ obtained in Ref.[25] within the Thomson and Spaepen approximation,[39] and $\lambda \sim 3$ Å, we get a crystal growth velocity of 10.9 m/s and 1.8 m/s at 700 K and 500 K respectively. These values agree very well with the numbers extracted from the direct simulations of the crystallization process (cf. Table 1), thus providing further verification of our previous results on homogeneous crystallization.[25]

Growth mechanism

The heterogeneous crystallization from the (100) surface is a rough, continuous growth, in which there are no preferential surface sites for the attachment of atoms from the liquid. We have observed no evidence of a layer by layer mechanism or of a birth and spread (two dimensional nucleation) process. In fact, the morphology of the growing surfaces shows a significant roughness at the atomic level, with a large number of under coordinated kink sites, evenly distributed across the model surface as shown in panel a) of Fig. 2. These and the following conclusions are drawn from the analysis of the model M2 characterized by the largest extension in the interface plane. Similar results are obtained for the smaller M1 model as reported in Fig. S3 of SI.

In order to discriminate between a layer-by-layer and a continuous 3D growth mechanism we have followed the approach of Ref.,[40] by dividing the simulation box into k slices along the growth axis. Each slice has a fixed thickness which is slightly larger than d_{hkl}, so that it can accommodate a complete crystalline plane. Then, we have computed the number of crystalline atoms $N_{c,k}$ contained in each k slice, and we have monitored $N_{c,k}$ as a function

of time for five k slices, starting from the outermost perfect crystalline one. The results reported in panel b) of Fig. 2 show that several k slices are growing at the same time at both 500 and 700 K, demonstrating that crystal growth proceeds in a continuous fashion without any evidence of lateral growth. Such a mechanism is due to the fact that the jump frequency of a single atom on the crystalline surface is lower than the rate of attachment per surface site of atoms from the melt. This can be assessed by computing the diffusion length that surface atoms (see SI for the definition) experience within the time interval t_l required to build a complete crystalline layer. From the growth velocities reported in Tab. 1, we obtain t_l=200 ps at 500 K and t_l=30 ps at 700 K. It turns out that within t_l only a small fraction ($\sim$ 8%) of surface atoms detaches from the crystalline surface and goes back to the liquid. The calculated 2D diffusion coefficient of surface atoms is $1.5 \pm 0.5 \cdot 10^{-8}$ cm^2/s and $1.7 \pm 0.2 \cdot 10^{-7}$ cm^2/s at 500 and 700 K, respectively. This implies that within t_l surface atoms move on average by $\sim$0.5 Å at both 500 and 700 K, a displacement much smaller than the average interatomic distance ($\sim$ 3.0 Å). Thus, we can conclude that for the majority of the atoms that stick onto the crystal growth front, surface diffusion is a much slower process with respect to the crystal growth at the interface, hence a surface roughness develops. Note that the diffusion coefficient of atoms in the melt away from the interface, calculated within a short time interval of 25 ps at 500 K and 5 ps at 700 K, is $D = 1.2 \cdot 10^{-6}$ and $1.0 \cdot 10^{-5}$ cm^2/s at 500 and 700 K respectively, which is consistent with the values computed in the homogeneous liquid.[24]

To investigate surface roughness, we have computed as a function of time the height-height correlation function

$$H(r_{xy}) = \langle [h(r_{xy} + r^0_{xy}) - h(r^0_{xy})]^2 \rangle \tag{3}$$

where $h(r_{xy})$ is the z coordinate of the surface at point r_{xy} and $\langle \dots \rangle$ stands for an average over the ensemble of the surface sites (see SI). To fit the height-height correlation function of the growing surface at each time instant we have used the following expression[42]

$$H(r_{xy}) = 2w_s^2 \left\{ 1 - e^{-\left(\frac{r_{xy}}{\xi}\right)^{2\alpha}} \right\}. \quad (4)$$

where α is the roughness exponent, ξ is the correlation length and w_s is the surface width. All these parameters depend on time during growth. To avoid overfitting we fixed the value of α to 0.7, as it oscillates in the range 0.6-0.8 and only affects the resulting values of ξ and w_s by an error of about $\sim$5%. The result of the fitting is shown in panel c) of Fig. 2, where we report the $H(r_{xy})$ function at different times within the interval in which the surface growth proceeds in a linear fashion (see Fig. 1). As $H(r_{xy})$ is clearly consistent with Eq. 4 along the whole linear regime, we can conclude that on the time and length scales probed by our simulations the growing surface has a finite roughness. The horizontal correlation length ξ increases with time as shown in panel d) of Fig. 2. As the resulting values of ξ are always shorter than half of the simulation box, we can trust the time evolution of w_s as well, which is shown in panel e) of Fig. 2. Since w_s clearly increases in time with a temperature dependent slope, we can not rule out the emergence of a kinetic roughening in the 500-700 K temperature range.

(111) surface

We now turn our attention to the case in which the crystalline phase exposes the (111) surface to the liquid (cf. Table 1). Both vapor-liquid-solid synthesis in vacuum[31] and super critical fluid-liquid-solid synthesis[32] produce octahedral shaped α-GeTe micro crystals that expose the surfaces corresponding to the (111) face of β-GeTe. The octahedral morphology might result from a lower surface free energy of the (111) face, particularly in the presence of the trigonal distortion which leads to the formation of three short and three long bonds. However, the predominance of the (111) face in the crystallites might be also related to the anisotropy in the crystal growth velocities. In fact, the surface with the lower growth speed will be more abundant. Thus, we have investigated the growth of the (111) surface as well

(model M111), to compare its growth speed with that of the (100) phase discussed in the previous section. It is not possible to predict which of the two surfaces grows faster on purely geometrical arguments. The inter planar spacing d_{111} is smaller than d_{100} ($d_{111} = d_{100} \cdot \frac{\sqrt{3}}{3}$) which would lead to a lower crystal growth velocity for the (111) surface, but on the other hand the number of broken bonds per atom is higher on the (111) surface than on the (100) which might increase the sticking on (111) and thus its growth speed. However, while the (100) surface exposes both atomic species in equal fraction, the {111} planes consist of hexagonal arrangements of either only Ge or only Te atoms. This chemical layering is expected to finally slow down the growth along the (111) direction with respect to the (100) as we have indeed observed in our simulations.

It has been recently reported[44] that the Te-terminated (111) GeTe surface is more stable than the Ge-terminated one. This feature is also confirmed by our simulations. In fact, we have initially built an interface model by terminating the (111) crystalline surfaces with Ge (top) or Te (bottom), but during the quenching protocol, from 1000 to 500 K, a complete Te-terminated new layer forms on top of the Ge-terminated surface, while nothing happens on top of the Te-terminated surfaces. This result provides further evidence of the stability of the Te-terminated (111) surface with respect to the Ge-terminated one. The comparison between the growth speeds u_{100} and u_{111} reported in Tab. 1 shows that indeed $u_{111} < u_{100}$ in this temperature range, although the difference is smaller at 700 K. We remark that at 500 K u_{100} and u_{111} have been obtained considering exclusively the linear regime of the crystal growth front, before nuclei from the melt start to interfere and thus growth from both the surface and the melt slows down as observed in the case of the (100) surface. A continuous mechanism for crystal growth is observed, analogously to the (100) surface (see the SI, Fig. S4), but for the fact that the (111) face roughens in a peculiar way. In fact, it turns out that the (111) surface grows by forming (100) facets, along which the crystal growth proceeds more rapidly, as depicted in Fig. 3. At 500 K, a large three sided pyramid exposing {100} planes forms on the timescale of about 2 ns, while crystal growth is negligible in the region

of the surface that still exposes the (111) plane, as depicted in Fig. 3. At 700 K, due to the larger atomic mobility, several smaller pyramids exposing the {100} planes can be found on top of the (111) growing surface. This feature can explain why the difference in the crystal growth speed is small at 700 K and becomes instead significant at 500 K. Thus, our results suggest that the growth of {100} planes is kinetically favored with respect to the {111} planes, which, besides thermodynamical considerations, would further favor the presence of the slow growing {111} faces in crystallites as observed experimentally. The same speed and mechanism of crystal growth have also been observed in a simulation of the (111) surface of the trigonal (α) phase of GeTe ($M111_T$, in Table 1). The crystal structure of α-GeTe can be seen as a trigonal distortion of the cubic phase along the [111] direction. The (111) plane of the trigonal phase thus corresponds to the (111) plane of the cubic one. Further details are reported in the SI (see Fig. S5).

Polycrystalline model

Phase change films in PCMs are actually deposited in polycrystalline form with grains size of the order of few tens of nanometers.[2] To better mimic PCMs conditions, we have generated a polycrystalline slab in contact with the supercooled liquid. The polycrystalline model (MP, cf. Table 1) was obtained from the homogeneous crystallization of a very large model of the supercooled liquid at 600 K where several nuclei form and grow at the same time in our simulations. Further details about the model and methods we have used to identify different grains are illustrated in the SI (Fig. S6 and S7). The polycrystalline interface contains eight distinct crystalline grains, randomly oriented and with sizes ranging from one to four nm, a configuration which is indeed very close to the real device. Luckily enough, two of the crystalline grains, C_{100} and C_{111}, expose the (100) and the (111) surface respectively, as depicted in panel a) of Fig. 4. Crystal growth is continuous also for the polycrystalline interface at 500 K and 700 K as found for the (100) surface (see the SI, Fig. S7). We do not observe a significant rearrangement of the grain boundaries on the ns timescale, even

at 700 K where mobility is higher. Each grain grows independently in a columnar fashion (see panels a) and b) of Fig. 4) until the top and bottom interfaces make contact. However the C_{100} and C_{111} grains also expand in the plane above neighboring grains characterized by other orientations which evidently grow at a lower pace. The crystalline-liquid interfacial area nearly doubles for the C_{100} (a factor 1.8) and C_{111} (a factor 1.9) grains. The in-plane expansion of the C_{111} grain follows the growth mechanism discussed in the previous section in which (100) facets are formed as depicted for the polycrystalline model in panel c) of Fig. 4. At 700 K the crystallization is nearly complete in 500 ps. The computed X-ray diffraction (XRD) patterns of the polycrystalline model and of the single crystal model M1 are very similar as shown in Fig. S6 in SI. The XRD peaks of the polycrystalline models are slightly broader to the the small crystallite sizes.

To extract the crystal growth velocity for the polycrystalline model, we have computed a density profile along the z axis, weighted by the $\bar{Q}_4$ local order parameter that quantifies the crystallinity of each atom (see SI). We have then obtained the position of the front of the crystallite growth following the prescriptions of Ref. 45, and tracked its progress in time as described in details in the SI. We have verified (see SI, Fig. S9) that in the case of the M1, M2 and M111 models this approach gives exactly the same results obtained in the previous sections. It turns out that the crystal growth velocity is lower for the polycrystalline model than for the (100) and (111) surfaces at both temperatures (cf. Table 1). This is expected because the adjustment of atoms at the grain boundaries is a slow process, as we have also observed in the presence of several growing crystalline nuclei in the simulations of homogeneous crystallization.[25]

Conclusions

We have investigated the heterogeneous crystallization of GeTe at the interface between the supercooled liquid and the crystalline phases at 500 and 700 K, two representative

temperatures of interest for actual PCM devices. It turns out that at 500 K, close to the glass transition temperature, homogeneous nucleation in the melt is a competitive process with respect to the heterogeneous crystallization from the interface, as the presence of the crystalline nuclei hinders the growth of the interface and the propagation of the crystalline front. The crystal growth velocity computed for the (100) crystalline surface is comparable to those obtained in the case of homogeneous growth from the melt. Indeed, our results confirm that in the 500-700 K range GeTe crystallization is diffusion-limited and can be properly described by classical nucleation theory. The heterogeneous crystal growth proceeds at both 500 and 700 K with a rough, continuous mechanism. The diffusion rate of crystalline atoms on the surface is lower than the rate of attachment per surface site of atoms from the melt, hence the interfaces develop a certain roughness in time, as quantified by the height-height correlation function. It turns out that the crystal growth front displays a finite roughness that grows with time, suggesting a possible kinetic roughening at 700 K. The same continuous growth mechanism holds at the (111) surface, though the latter grows slower than the (100). In fact, the (111) surface tends to facet with time by exposing {100} facets, more or less extended depending on temperature, along which crystallization rapidly proceeds. The faster growth of the {100} planes with respect to the {111} planes could be an additional, kinetic motivation for the the presence of the slow growing (111) faces in GeTe micro-crystals. Finally, we built a polycrystalline interface made of different grains, a configuration extremely close to the actual geometry of the PCM devices. It turns out that no grain boundary rearrangements takes place on the ns timescale. Each grain grows more or less independently in a columnar fashion with an overall growth velocity lower than both the (100) and (111) surfaces. The temperature dependence of the crystal growth velocity in the temperature range 500-700 K is mostly controlled by the atomic diffusivity in the supercooled liquid phase.

Supporting Information Available

We provide supporting information (SI) on the results of the heterogeneous crystallization of the phase change material GeTe.

This material is available free of charge via the Internet at `http://pubs.acs.org/`.

Acknowledgement

We thankfully acknowledge the computational resources provided by Cineca (Casalecchio di Reno, Italy) through the program EU-FP7 Prace and by the Swiss National Supercomputing Centre (CSCS) under Project No. s510. M.P. acknowledges funding from the Swiss National Science Foundations through the project NCCR MARVEL n.51NF40_141828. M.B. acknowledges funding from the European Union Seventh Framework Programme (FP7/2007-2013) under grant agreement n. 310339. We thank G. Miceli for his contribution to the early stage of this work and D. Campi for his involvement with the revision of the manuscript.

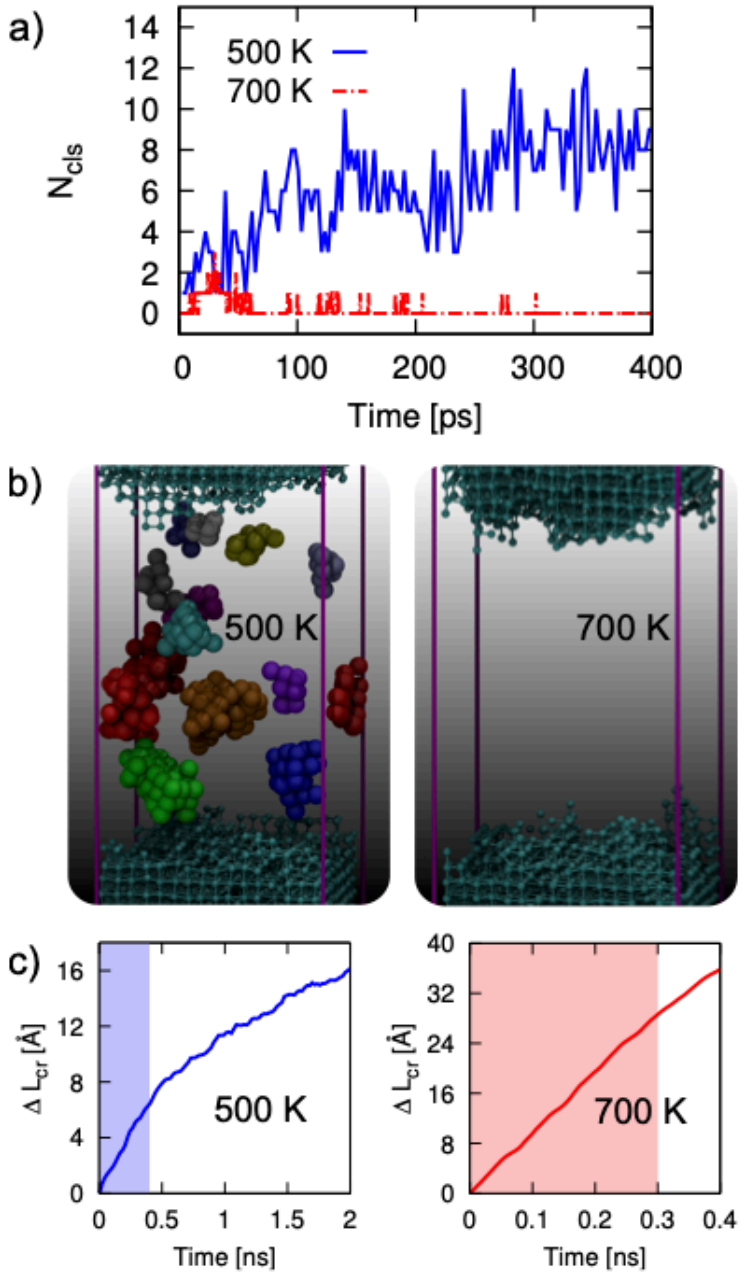

Figure 1: a) Number of crystalline clusters of size larger than eight atoms as a function of time within the supercooled liquid phase. b) Representative snapshots from simulations at 500 and 700 K. Only crystalline atoms are shown. Atoms belonging to the crystalline surface are depicted in a ball-and-sticks fashion (light blue), while each crystalline nucleus in the melt is shown in a different color. Liquid-like atoms fill the space between the two growing surfaces at the edges of the simulation cell depicted in purple. Periodic boundary conditions in the three dimensions are applied. c) Linear dimension of the crystal growth front ($L_{cr}(t) - L_{cr}(t_0)$, see text) as a function of time at 500 and 700 K. The red/blue regions mark the time lags in which the crystal growth proceeds in a linear fashion. All the data reported in this picture refer to model M1.

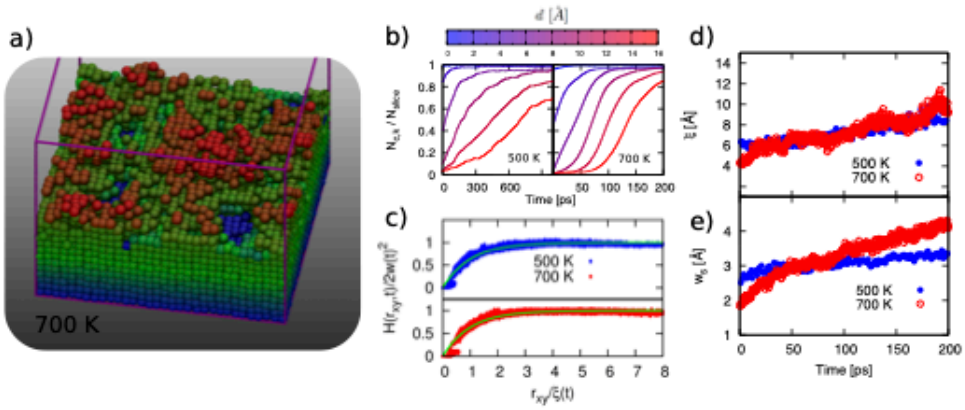

Figure 2: a) Snapshot of the rough crystalline (bottom) surface at 700 K, taken at t=100 ps. Only crystalline atoms, colored according to their z-coordinate, are shown. b) Number of crystalline atoms belonging to the surface in each k slice ($N_{c,k}$, see text) normalized by the number of crystalline atoms in a perfect crystalline layer N_{slice} as a function of time at 500 and 700 K. The color map refers to the distance d of the k slice from the outermost perfect crystalline layer. c) Height-height correlation function (see text) as a function of time at 500 and 700 K, scaled by the factors $s_H = 0.5w(t)^{-2}$ on the y-axis and $s_r = \xi(t)^{-1}$ on the x-axis. The solid green lines refer to the functional form in Eq. 4 with α=0.7. d) Horizontal correlation length ξ and e) surface width w_s as a function of time at 700 and 500 K, shown within the time interval during which the crystal growth is linear in time. All the data presented in this figure refer to the model M2.

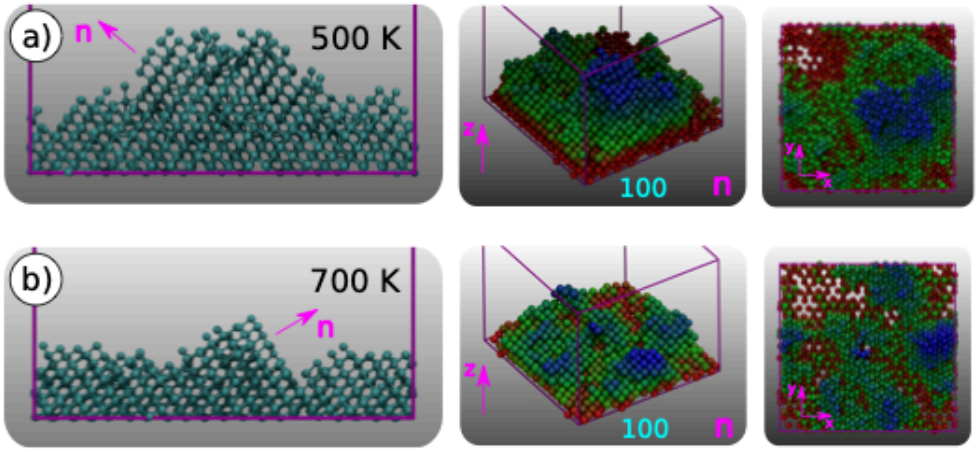

Figure 3: a) Snapshot of the (111) surface morphology during crystal growth at 500 K. Only crystalline atoms belonging to the growing (bottom) surface are depicted. The same configuration is shown projected onto the xz plane (left), along the normal n at one of the {100} planes formed (middle), and onto the xy plane (right). Atoms are colored according to their z coordinate in middle and right panels. b) Same as above at 700 K.

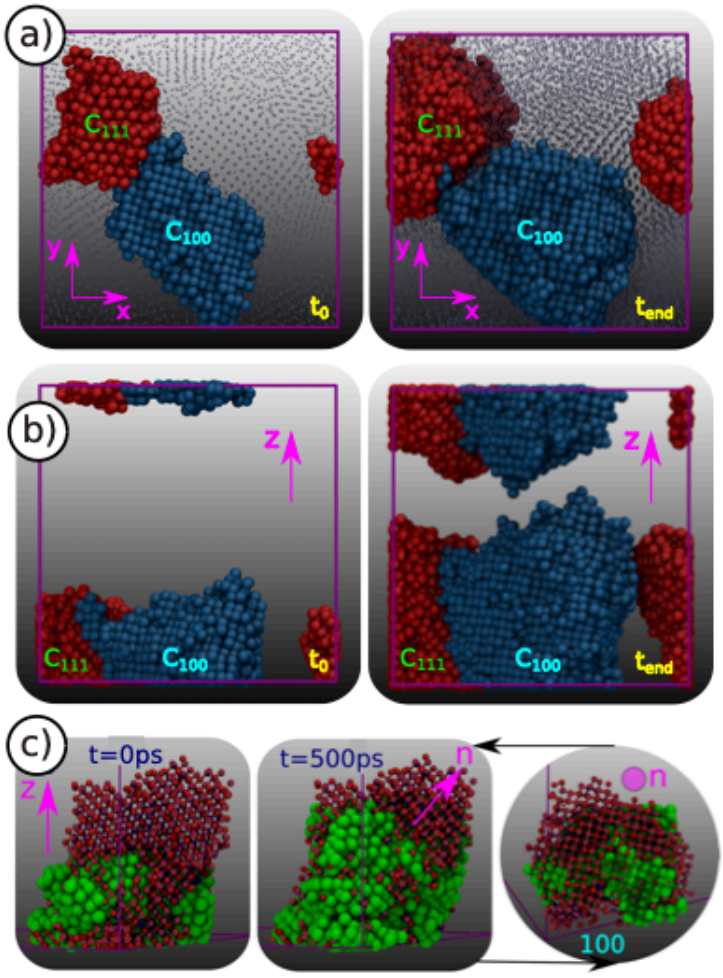

Figure 4: a) C_{111} (red) and C_{100} (blue) crystalline grains in the MP polycrystalline model at the beginning (t_0) and at the end (t_{end}) of the crystallization simulation. Projections along the xy planes are shown. b) Same as above, but this time the snapshots are projected along the xz plane. c) Anisotropic growth of C_{111} along the $\langle 100 \rangle$ direction. Red balls depict the final configuration at t=500 ps, while green balls follow the temporal evolution. The inset on the right shows the same configuration viewed along the normal n to a (100) plane.

References

(1) Wuttig, M.; Yamada N. Phase-Change Materials for Rewriteable Data Storage. *Nat. Mater.* **2007**, *6*, 824-832.

(2) Lencer, D.; Salinga, M.; Wuttig, M. Design Rules for Phase-Change Materials in Data Storage Applications. *Adv. Mat.* **2011**, *23*, 2030-2058.

(3) Pirovano, A.; Lacaita, A.L.; Benvenuti, A.; Pellizzer, F.; Bez, R. Electronic Switching in Phase-Change Memories. *IEEE Trans. Electron. Dev.* **2004**, *51*, 452-459.

(4) Lacaita, A.L.; Redaelli, A. The Race of Phase Change Memories to Nanoscale Storage and Applications. *Microelec. Eng.* **2013**, *109*, 351-356.

(5) Salinga, M.; Wuttig, M. Phase-Change Memories on a Diet. *Science* **2011**, *332*, 543-544.

(6) Kuzum, D.; Jeyasingh, R.G.D; Lee, B.; Wong, H.W.P. Nanoelectronic Programmable Synapses Based on Phase Change Materials for Brain-Inspired Computing. *Nano Lett.* **2012**, *12*, 2179-2186.

(7) Wright, C.D.; Liu, Y.; Kohary, K.I.; Aziz, M.M.; Hicken, R.J. Arithmetic and Biologically-Inspired Computing Using Phase-Change Materials. *Adv. Mat.* **2011**, *23*, 3408-3413.

(8) Loke, D.; Lee, T.H.; Wang, W.J, Shi, L.P.; Zhao, R.; Yeo, Y.C.; Chong, T.C.; Elliott, S.R. Breaking the Speed Limits of Phase-Change Memory. *Science* **2012**, *336*, 1566-1569.

(9) Raoux S.; Welnic W.; Ielmini D. Phase Change Materials and Their Application to Nonvolatile Memories. *Chem. Rev.* **2010**, *110*, 240-267.

(10) Orava, J.; Greer, A.L.; Gholipour, B.; Hewak D.W.; Smith, C.E. Characterization of Supercooled Liquid Ge2Sb2Te5 and its Crystallization by Ultrafast-heating Calorimetry. *Nat. Mat.* **2012**, *11*, 279-283.

(11) Jeyasingh, R.; Fong S.W.; Lee J.; Li Z.; Chang K.; Mantegazza D.; Asheghi M.; Goodson K.E.; Wong H.P. Ultrafast Characterization of Phase-Change Material Crystallization Properties in the Melt-Quenched Amorphous Phase. *Nano Lett.* **2014**, *14*, 3419-3426.

(12) Ciocchini, N.; Cassinerio, M.; Fugazza, D.; Ielmini, D. Evidence for Non-Arrhenius Kinetics of Crystallization in Phase Change Memory Devices. *IEEE Trans. Elec. Dev.* **2013**, it 60, 3767-3774.

(13) Hegedüs; J.; Elliott, S.R. Microscopic Origin of the Fast Crystallization Ability of GeSbTe Phase-Change Memory Materials. *Nat. Mater.* **2008**, *7* 399-405.

(14) Lee, T.H.; Elliott, S.R. Ab Initio Computer Simulation of the Early Stages of Crystallization: Application to Ge2Sb2Te5 Phase-Change Materials. *Phys. Rev. Lett.* **2011**, *107*, 145702.

(15) Kalikka, J.; Akola, J.; Jones, R. O. Simulation of Crystallization in $Ge_2Sb_2Te_5$: A Memory Effect in the Canonical Phase-chnage Material. *Phys. Rev. B* **2014**, *90*, 184109-9.

(16) Behler, J.; Parrinello, M. Generalized Neural-Network Representation of High-Dimensional Potential-Energy Surfaces. *Phys. Rev. Lett.* **2007**, *98*, 146401.

(17) Behler, J. Atom-centered Symmetry Functions for Constructing High-dimensional Neural Network Potentials. *J. Chem. Phys.* **2011**, *134*, 074106-13.

(18) Behler, J. Representing Potential Energy Surfaces by High-dimensional Neural Network Potentials. *J. Phys. Cond. Matt.* **2014**, *26*, 183001.

(19) Sosso, G.C.; Miceli, G.; Caravati, S.; Behler, J.; Bernasconi, M. Neural Network Interatomic Potential for the Phase-Change Material GeTe. *Phys. Rev. B* **2012**, *85*, 174103.

(20) Sosso, G.C.; Donadio, D.; Caravati, S.; Behler, J.; and Bernasconi, M. Thermal Transport in Phase-change Materials from Atomistic Simulations. *Phys. Rev. B* **2012**, *86*, 104301-5.

(21) Akola, J.; Jones R.O. Structural Phase Transitions on the Nanoscale: The Crucial Pattern in the Phase-change Materials Ge2Sb2Te5 and GeTe. *Phys. Rev. B.* **2007**, *76*, 235201-10.

(22) Caravati, S.; Bernasconi, M.; Kühne T.D.; Krack, M.; Parrinello, M. Coexistence of Tetrahedral- and Octahedral-like Sites in Amorphous Phase Change Materials. *App. Phys. Lett.* **2007**, *91*, 171906.

(23) Mazzarello, R.; Caravati, S.; Angioletti-Uberti, S.; Bernasconi, M.; Parrinello, M. Signature of Tetrahedral Ge in the Raman Spectrum of Amorphous Phase-Change Materials. *Phys. Rev. Lett.* **2011**, *104*, 085503.

(24) Sosso, G.C.; Behler, J.; Bernasconi, M. (2012) Breakdown of Stokes-Einstein Relation in the Supercooled Liquid State of Phase Change Materials. *Physica Status Solidi B* **2013**, *249*, 1880-1885; erratum *250*, 1453 .

(25) Sosso, G.C.; Miceli, G.; Caravati, S.; Giberti, F.; Behler, J.; Bernasconi, M. Fast Crystallization of the Phase Change Compound GeTe by Large-Scale Molecular Dynamics Simulations. *J. Phys. Chem. Lett.* **2013**, *4*, 4241-4246.

(26) Sosso, G.C.; Colombo, J.; Behler, J.; Del Gado, E.; Bernasconi, M. Dynamical Heterogeneity in the Supercooled Liquid State of the Phase Change Material GeTe *J. Phys. Chem. B* **2014**, *118*, 13621-13628.

(27) Bruns, G.; Merkelbach, P.; Schlockermann, C.; Salinga, M.; Wuttig, M.; Happ, T.D.; Philipp, J.B.; Kund, M. Nanosecond Switching in GeTe Phase Change Memory Cells. *Appl. Phys. Lett.* **2009**, *95*, 043108.

(28) Raoux, S.; Cheng, H.Y.; Caldwell, M.A.; Wong, H-S.P Crystallization times of GeTe Phase Change Materials as a Function of Composition. *Appl. Phys. Lett.* **2009**, *95*, 071910.

(29) A. Bastard *et al.* Crystallization Study of "Melt Quenched" Amorphous GeTe by Transmission Electron Microscopy for Phase Change Memory Applications. *Appl. Phys. Lett.* **2011**, *99*, 243103.

(30) Klemm, W.; Frischmuth, G. Das System Germanium-Tellur. *Z. Anorg. Chem.* **1934**, *218*, 249-251.

(31) Chung, H.; Jung, Y.; Kim, S.C.; Kim, D.H, Oh, K.H.; Agarwal R. Epitaxial Growth and Ordering of GeTe Nanowires on Microcrystals Determined by Surface Energy Minimization. *Nano Letters* **2009**, *9*, 2395-2401.

(32) Tuan, H.; Korgel, B.A. Aligned Arrays of Te Nanorods Grown from the Faceted Surfaces of Colloidal GeTe Particles. Crys. Growth Des. **2008**, *8*, 2555-2561.

(33) Goldak, J.; Barrett, C.S.; Innes, D.; Youdelis, W. The Structure of αGeTe. *J. Chem. Phys.* **1966**, *44*, 3323-3325.

(34) Raoux, S.; Munoz, B.; Cheng, H.Y.; Jordan-Sweet, J.L. Phase Transitions in Ge-Te Phase Change Materials Studied by Time- Resolved X-ray Diffraction. *Appl. Phys. Lett.* **2009**, *95*, 143118.

(35) Chattopadhyay, T.; Boucherle, J.X.; Von Schnering, H.G. Neutron Diffraction Study on the Structural Transition in GeTe. *J. Phys. C Sol. State Phys.* **1987**, *20*, 1431.

(36) Fons, P.; Kolobov, A.V.; Krbal, M.; Tominaga, J.; Andriakopoulos, K.S.; Yannopoulos, S.N.; Voyiatzis, G.A.; Uruga, T. Phase Transition in Crystalline GeTe: Pitfalls of Averaging Effects. *Phys. Rev. B* **2010**, *82*, 155209.

(37) Wilson, H.A. On the Velocity of Solidification and Viscosity of Super-cooled Liquids. *Phil. Mag.* **1900**,*50*, 238-250.

(38) Frenkel, Y. The Kinetic Theory of Liquids. *Oxford University Press* (1946).

(39) Thomson, C.V.; Spaepen, F. On the Approximation of the Free Energy Change on Crystallization. *Acta Metall.* **1979**, *27*, 1855-1859.

(40) Salvalaglio, M.; Vetter, T.; Giberti, F.; Mazzotti, M.; Parrinello, M. Uncovering Molecular Details of Urea Crystal Growth in the Presence of Additives. *J. Am. Chem. Soc.* **2012**, *134*, 17221-17233.

(41) Pelliccione, M.; Lu T-M Evolution of Thin Film Morphology (Springer, 2008).

(42) Salditt, T.; Metzger, T.H.; Brandt, C.; Klemradt, U.; Peisl J. Determination of the Static Scaling Exponent of Self-affine Interfaces by Nonspecular X-ray Scattering. *Phys. Rev. B* **1995**, *51*, 5617-5627.

(43) Herlach, D.M. (ed) Solidification and Crystallization (Wiley-VCH Verlag GmbH, 2006).

(44) Deringer, V.L.; Lumeij, M.; Dronskowski R. Ab Initio Modeling of α-GeTe(111) Surfaces. *J. Phys. Chem. C* **2012**, *116*, 15801-15811.

(45) Hayward, J.A.; Haymet, A.D.J. The ice/water interface: Molecular Dynamics Simulations of the Basal, Prism, $\{20\bar{2}1\}$, and $\{2\bar{1}\bar{1}0\}$ Interfaces of ice Ih. *J. Chem. Phys.* **2011**, *114*, 3713-3726.

SUPPORTING INFORMATION

Heterogeneous Crystallization of the Phase Change Material GeTe via Atomistic Simulations

Gabriele C. Sosso,[*,†,‡] *Matteo Salvalaglio,*[†,‡,¶] *Jörg Behler,*[§] *Marco Bernasconi,*[‖] *and Michele Parrinello*[†,‡]

Department of Chemistry and Applied Biosciences, ETH Zurich, Vladimir-Prelog-Weg 1-5 CH-8093 Zurich, Switzerland, Faculty of Informatics, Università della Svizzera Italiana, Via G. Buffi 13, CH-6900 Lugano, Switzerland, Institute of Process Engineering, ETH Zurich, Sonneggstrasse 3, CH-8092 Zurich, Switzerland, Lehrstuhl für Theoretische Chemie, Ruhr-Universität Bochum, Universitätsstrasse 150, D-44780 Bochum, Germany, and Dipartimento di Scienza dei Materiali, Università di Milano-Bicocca, Via R. Cozzi 55, I-20125 Milano, Italy

E-mail: gabriele.sosso@phys.chem.ethz.ch

[*]To whom correspondence should be addressed
[†]ETH Zurich
[‡]Università della Svizzera Italiana
[¶]ETH Zurich
[§]Ruhr-Universität Bochum
[‖]Università di Milano-Bicocca

We provide supplementary information on the results concerning the crystal growth of GeTe phase change material.

MD simulations. Molecular dynamics simulations have been carried out using the DL_POLY[1] simulation package, interfaced with the Neural Network code RuNNer.[2] The time step for the numerical integration of the equations of motion has been set to 2 fs, and the canonical NVT ensemble has been sampled via the Bussi-Donadio-Parrinello stochastic thermostat .[3] Interfaces between crystalline and supercooled liquid GeTe have been built by merging models of crystal and liquid GeTe, equilibrated according to the following protocol: at first, 10 ps long simulations have been run at 1000 K, a temperature very close to the both the experimental and the theoretical melting temperatures of 998[4] and 1023 K;[5] crystalline atoms have been kept fixed at this stage, a constraint that has been removed in the subsequent quenching simulations, in which the interface has been brought from 1000 to 500 K in 50 ps; production runs of crystallization have been started after 25 ps of equilibration at 500 K. Crystallization at 700 K has been investigated by using the same interfaces as above, heated in 25 ps from 500 to 700 K, and equilibrated at the latter temperature for 25 ps before starting the crystallization production runs. This protocol has allowed to obtain realistic interfaces with a finite roughness. The initial models of the crystal and liquid phase of GeTe were generated according to Ref. 6 at the theoretical equilibrium densities of 0.0357 and 0.0335 atoms/Å^3 respectively. Since the simulations were performed at fixed volume of the supercell, voids are formed during crystallization of the liquid as indeed occurs in the device. The effect of density of the liquid in the crystallization speed has been analyzed for the homogeneous case in our previous work .[6] A similar decrease in the crystallization speed upon increase of the density is expected to be present here for the heterogeneous crystallization. The polycrystalline sample has been obtained as follows: we have taken a model of the supercooled liquid and let it crystallize at 600 K, where different critical nuclei pop up from the melt and grow simultaneously.[6] We have then cut a slab along a direction perpendicular

to one of the edges of the cubic box, obtaining a polycrystalline sample (about 5 grains) that exposes different crystal surfaces. The interface between the polycrystalline sample and the supercooled liquid has been created as above.

(100) surface. In Fig. S1 we report for the M2 model the number of crystalline clusters at 500 and 700 K, a representative snapshot that depicts the crystalline nuclei in the melt at 500 K, and the linear dimension of the crystal growth front as a function of time at 500 and 700 K, together with the total fraction of crystalline atoms. These results are consistent with what we have obtained in the case of the M1 model (see main text), and provide further evidence of the absence of finite size effects.

In Fig. S2 we describe the temporal evolution of the fraction of crystalline atoms with respect to the whole system for both M1 and M2 at 500 and 700 K.

In Fig. S3 we show for the M1 model a representative snapshot of the rough crystalline (bottom) surface at 700 K, taken at t=100 ps, the number of crystalline atoms in each k slice (see main text) at 500 and 700 K as a function of time, the height-height correlation function at each instant within the linear regime at both 700 and 500 K, and the time evolution of both the horizontal correlation length ξ and the width w_s of the surface as a function of time (see main text).

(111) surface and MP model. In Fig. S4 we show for the M111 and the MP model the the number of crystalline atoms in each k slice (see main text) at 500 and 700 K as a function of time. In the case of M111, an initial transient in which the growth is slower can be observed. This is possibly due to the fact that the M111 surfaces have to build a certain roughness before being able to expose the fast growing (100) planes. In the case of the MP model, a significant rearrangements of the atoms within the polycrystalline slab and its interface takes place, possibly due to the crystallization of amorphous spots still present in the slab and to coarsening of the different crystalline grains.

In Fig. S5 we report selected results for the model M111$_T$. This model exposes the (111) surface (trigonal notation) of the trigonal distorted crystalline phase of GeTe. In the absence of the trigonal distortion, this surface reduces to the (111) surface of the cubic phase. In panel a) we show the time evolution of the number of crystalline nuclei in the melt, which as expected is not affected by the morphology of the interface. In panel b) a representative snapshot of the (bottom) crystalline surface is shown. Although the model is relatively small, it can be clearly seen that the surface tends to expose (100) - cubic notation - facets. Finally, we report in panel c) the evolution of the linear dimension of the crystal growth front with time.

Order parameter. In order to assess whether an atom i belongs to the crystal or the liquid phase, we have employed the averaged local order parameter $\bar{q}_{4m}(i)$ described in Ref. 7 to build an order parameter $\bar{Q}_4(i)$ as

$$\begin{aligned}
\bar{Q}_4(i) &= \frac{1}{N_b(i)} \sum_{j=1}^{N_b(i)} \frac{\sum_{m=-4}^{4} \bar{q}_{4m}(i)\bar{q}_{4m}(j)^*}{(\sum_{m=-4}^{4} |\bar{q}_{4m}(i)|^2)^{1/2}(\sum_{m=-4}^{4} |\bar{q}_{4m}(j)|^2)^{1/2}} \\
\bar{q}_{4m}(i) &= \frac{1}{\hat{N}_b(i)} \sum_{k=0}^{\hat{N}_b(i)} q_{4m}(k) \\
q_{4m}(k) &= \frac{1}{N_b(k)} \sum_{l=1}^{N_b(k)} Y_{4m}(\hat{\mathbf{r}}_{kl})
\end{aligned} \tag{1}$$

where j runs over the $N_b(i)$ neighboring atoms, k runs over the $\hat{N}_b(i)$ neighboring atoms including the i-th atoms itself, and $Y_{4m}(\hat{\mathbf{r}}_{kl})$ are the spherical harmonics of the polar angles defined by the versor $\hat{\mathbf{r}}_{kl}$ which links atoms i and j. The neighboring $N_b(i)$ atoms include the first coordination shell of crystalline GeTe at its theoretical equilibrium density. We define as crystalline an atom with $\bar{Q}_4$ greater than 0.9 (Fig. S6), and we consider two crystalline atoms as connected up to a cutoff distance of 3.6 Å. In Fig. S6 we plot the probability density distribution of the order parameter $\bar{Q}_4$ for the M1 model at 700 K at the beginning,

middle and end of the crystallization (t=0, 200 and 400 ps). It is clear that such an order parameter is able to distinguish very sharply between the crystalline and disordered phases even in the presence of diffuse interfaces such the ones we are dealing with in our simulations. A representative snapshot is also shown.

Polycrystalline model analysis. The quantitative analysis of the growth of the polycrystalline model has required special care. One of the qualities of the order parameters used to define the state of individual atoms in the simulation box is rotational invariance. It is clear then that the same order parameter does not allow for a neat distinction between crystalline domains (grains) with different spatial orientation. To identify different grains we analyze the orientation of the local environment of each atom in a crystal like configuration as follows. For each i-th atom we define a vector $\overrightarrow{v_i}$ oriented along the segment joining the atom and its farthest neighbor within a cutoff of 3.6 Å. In such a way, directionality information is attached to each atom in a crystal-like configuration. To distinguish the largest crystal grains in the simulation box we compute $h(\theta_x, \theta_y, \theta_z)$, the three dimensional histogram of the angles described by the vectors $\overrightarrow{v_i}$ with the three unitary vectors defining the orientation of the x, y, and z. Local maxima in $h(\theta_x, \theta_y, \theta_z)$, identify highly probable local orientations, e.g. large groups of atoms with similar orientation $\overrightarrow{v_i}$. Grains are identified as clusters of crystalline atoms belonging to the same histogram peak in the space $h(\theta_x, \theta_y, \theta_z)$. We remind that the histogram is built on top of the subset of the crystalline atoms only, previously classified according the $\bar{Q}_4$ order parameter.

In Fig. S7 we report a projection of the $h(\theta_x, \theta_y, \theta_z)$ three dimensional histogram on the θ_x, θ_z plane. Thanks to this approach we are able to effectively pinpoint the different grains within the polycrystalline model MP and to keep track of them during crystallization, as depicted in a representative snapshot.

In Fig. S8 we report the XRD pattern of cubic GeTe. The XRD pattern for ideal c-GeTe at 0 K has been obtained via the CrystalMaker and CrystalDiffract softwares. The XRD

patterns for the fully crystallized M1 and MP models at 700 K has been obtained instead with the Debyer software (https://code.google.com/p/debyer/), specifically designed to deal with disordered structures like e.g. our polycrystalline model. X-ray source wavelength has been set to λ=1.541 Å in all cases. The XRD patterns of M1 and MP at 700 K look similar, as Debye thermal broadening plays an important role at such an high temperature. In agreement with the suggestions by Krbal *et al.*,[8] the small domains size (1-4 nm) of the polycrystalline model MP results in slightly broader XRD peaks with respect to M1 (single crystal). However, the effect of the crystalline domains size is blurred in here by both Debye thermal broadening and the presence in the MP model of a small fraction of still disordered material at the grain boundaries.

In Fig. S9 we show the density profile $\rho(z_k)$ of the M2 model at 700 K, weighted by the order parameter $\bar{Q}_4$:

$$\rho(z_k) = \frac{1}{N}\sum_{i=1}^{N}\left[\exp -\frac{(r_z^i - z_k)^2}{\sigma_k}\right]\cdot \bar{Q}_4^i \tag{2}$$

where r_z^i is the z coordinate of the atom i, z_k is the value of the z coordinate along a reference mesh and σ_z is a parameter that tunes the profile resolution along the z coordinate. Following the approach described in Ref. 9, we have applied a Gaussian filter in the reciprocal space from which we have obtained the smooth, filtered $\rho^*(z_k)$ profile also reported in Fig. S9. By taking the first derivative of the latter with respect to z_k we can easily track the behavior of the crystal growth front as a function of time. In panel b) of Fig. 9 we plot the results obtained for the MP model and the M2 model. Hence, we can make a comparison of the crystal growth speed extracted by Eq.(3) in the main text and the approach explained in here. The results obtained by two methods are in remarkable agreement.

Surface atoms. Quantifying the crystal surface roughness requires the definition of a surface which moves in time according to the crystal growth front. To this end, at each time t we have built a regular grid in the xy plane with a spacing of 2.5 (small enough to accommodate

a single surface site in a unique bin of the grid), selecting for each point of the mesh the atom of the crystalline slab with the highest z coordinate (or lowest for the bottom surface). The set $N_s(t)$ of these atoms has then been used to compute both the diffusion coefficient of the surface atoms, $D(N_s(t))$, and the height-height correlation function $H(r_{xy}, t)$.

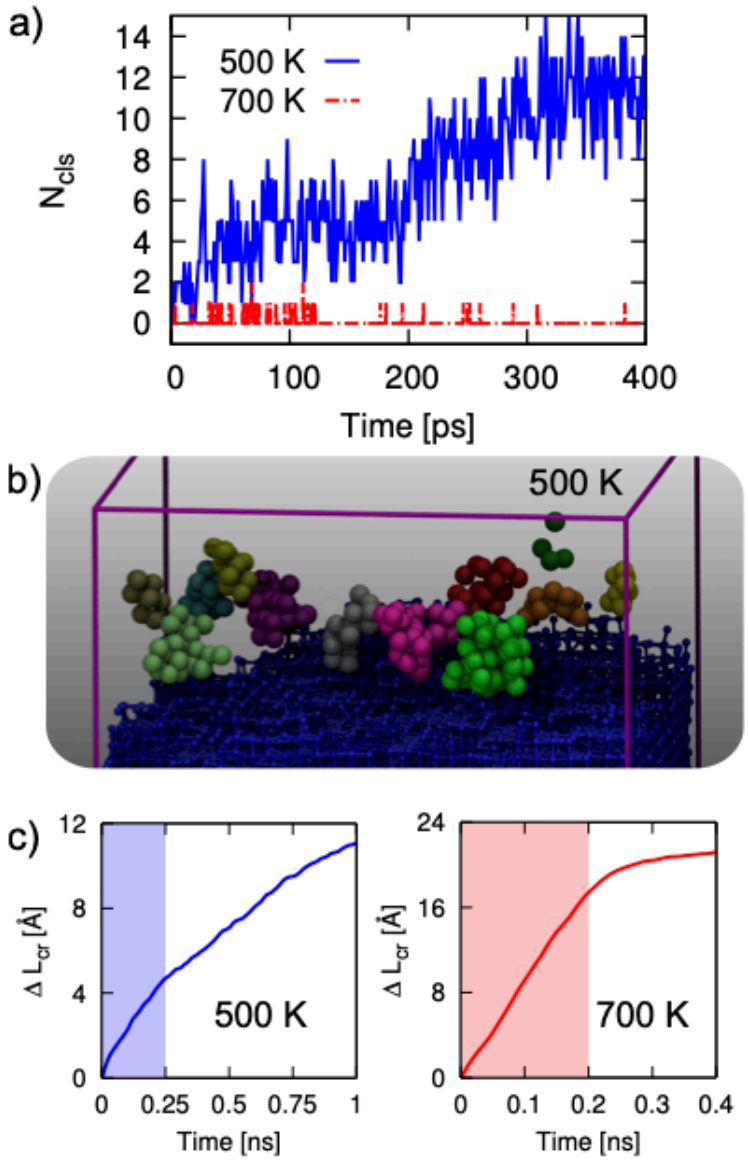

Fig. S1: a) Number of crystalline clusters of size larger than eight atoms as a function of time within the supercooled liquid phase. b) Snapshots from simulations at 500 K. Only crystalline atoms are shown. c) Linear dimension of the crystal growth front ($L_{cr}(t) - L_{cr}(t_0)$, see main text) as a function of time at 500 and 700 K. The red/blue regions mark the time lags in which the crystal growth proceeds in a linear fashion. All the data reported in this picture refer to model M2.

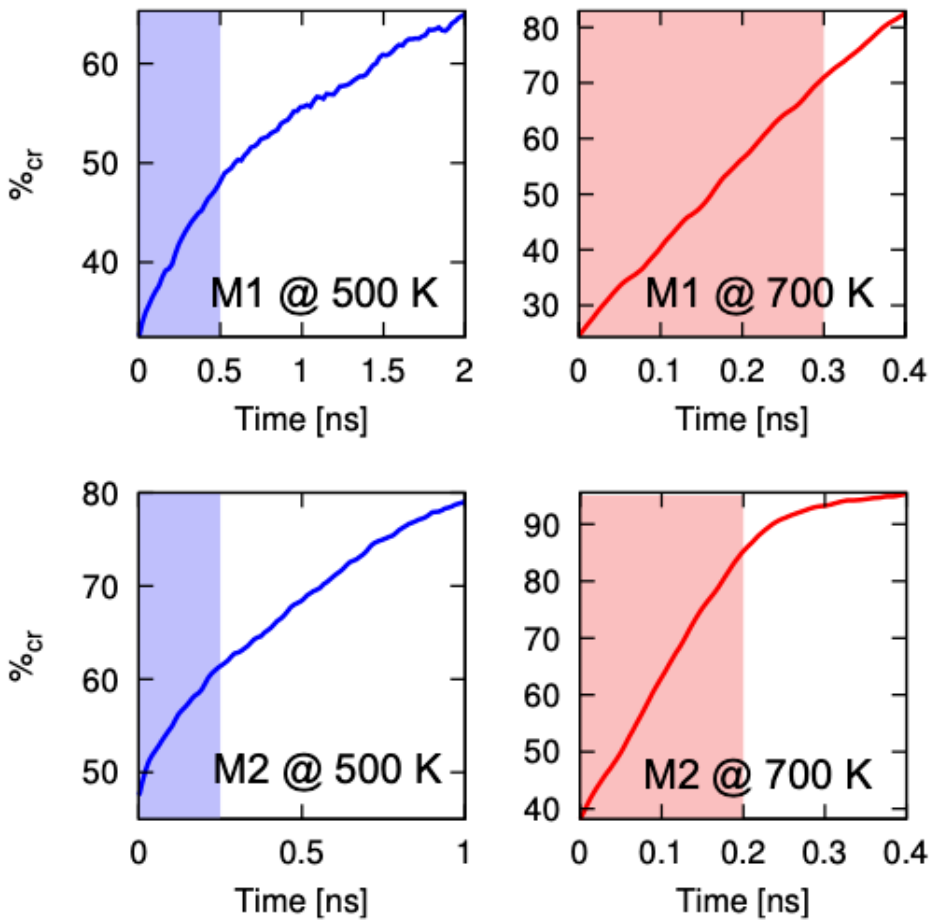

Fig. S2: Fraction of crystalline atoms with respect the whole system as a function of time, reported for both M1 and M2 at 500 and 700 K. The red/blue regions mark the time lags in which the crystal growth proceeds in a linear fashion.

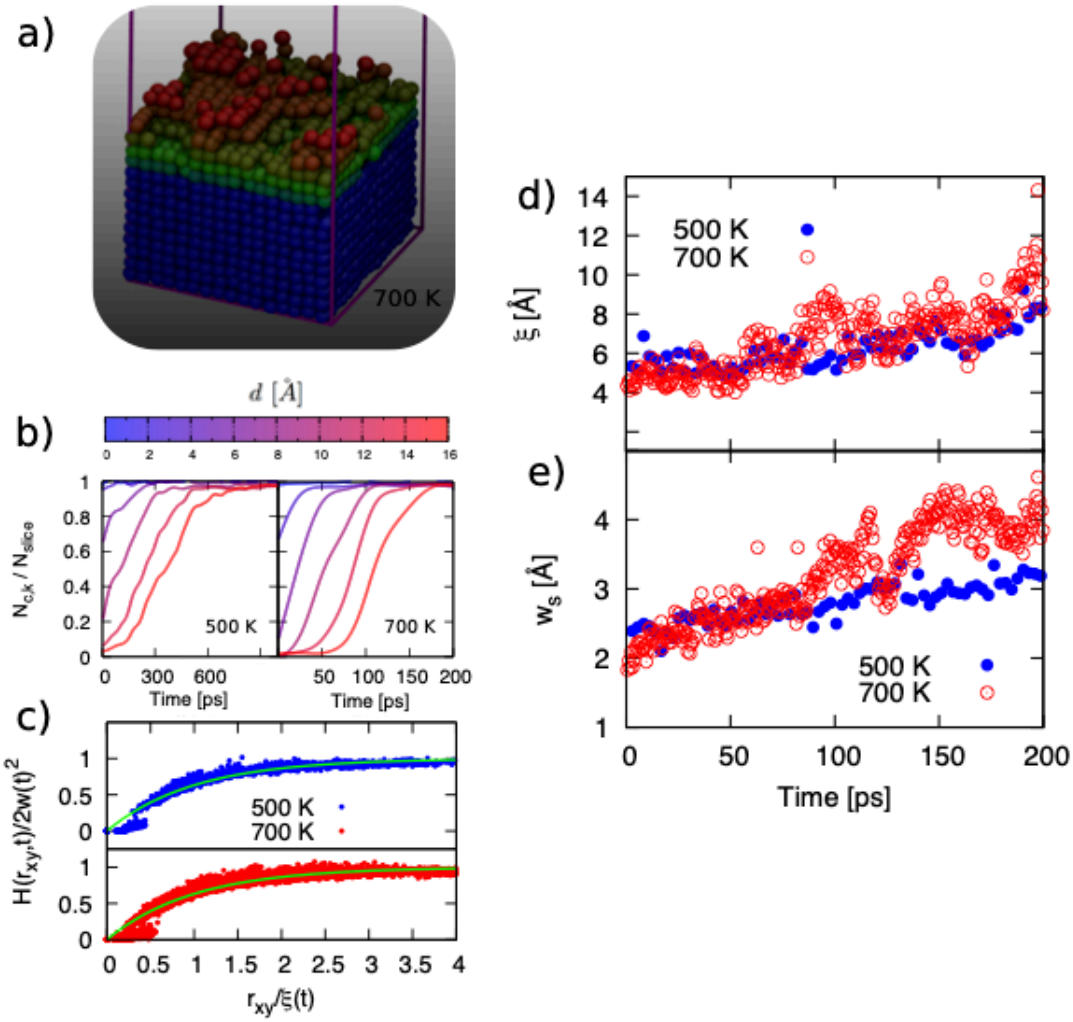

Fig. S3: a) Snapshot of the rough crystalline (bottom) surface at 700 K, taken at t=100 ps. Atoms are colored according to their z-coordinate. b) Number of crystalline atoms belonging to the surface in each k slice ($N_{c,k}$, see text) normalized by the number of crystalline atoms in a perfect crystalline layer N_{slice} as a function of time at 500 and 700 K. The color map refers to the distance d of the k slice from the outermost perfect crystalline layer. c) Height-height correlation function (see text) as a function of time at 500 and 700 K, scaled by the factors $s_H = 0.5w(t)^{-2}$ on the y-axis and $s_r = \xi(t)^{-1}$ on the x-axis. The solid green lines refer to the functional form in Eq. (4) in the main text with α=0.7. d) Horizontal correlation length ξ and e) surface width w_s as a function of time at 700 and 500 K, shown within the time interval during which the crystal growth is linear in time. All the data presented in this figure refer to the model M1.

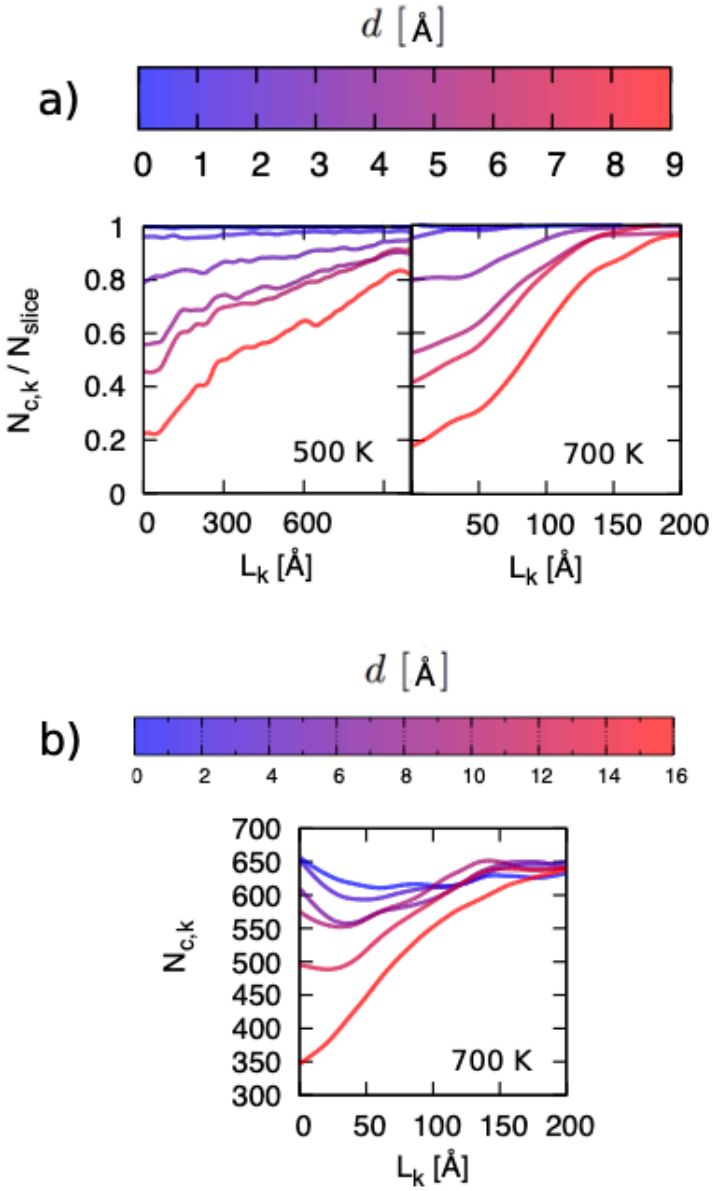

Fig. S4: a) Number of crystalline atoms belonging to the surface in each k slice ($N_{c,k}$, see main text) normalized by the number of crystalline atoms in a perfect crystalline layer N_{slice} as a function of time reported for M111 at 500 and 700 K. The color map refers to the distance d of the k slice from the outermost perfect crystalline layer. b) As above, this time reported for MP at 700 K without the N_{slice} normalization factor.

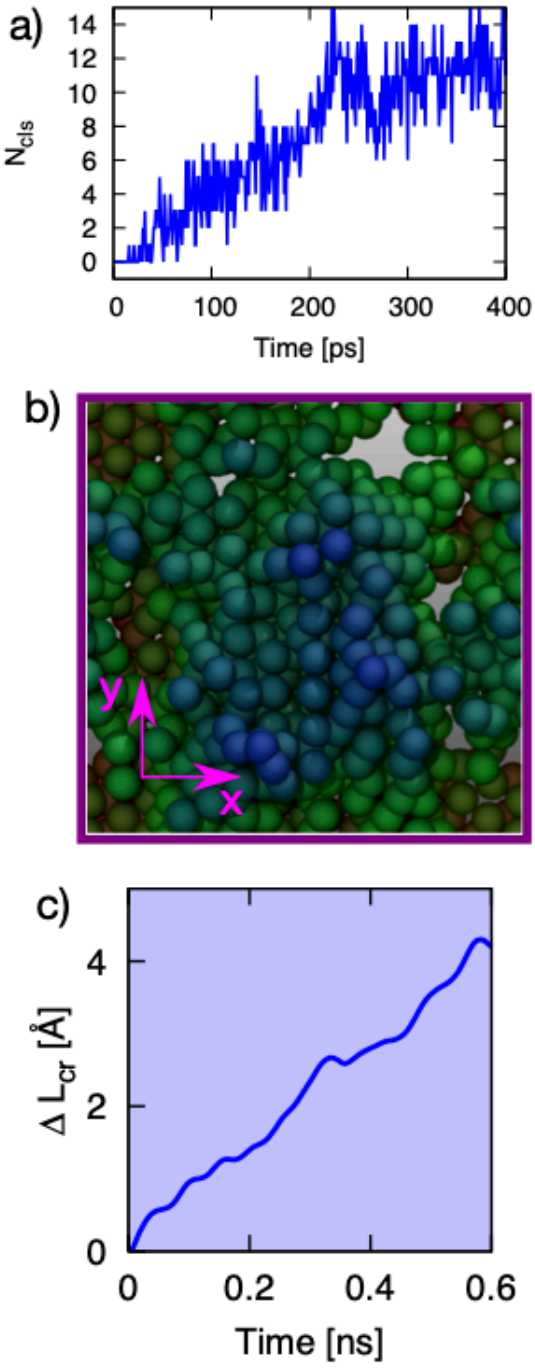

Fig. S5: Crystallization at the (111) surface of the trigonal GeTe crystal at 500 K (model $M111_T$). a) Number of crystalline clusters of size larger than eight atoms as a function of time within the supercooled liquid phase. b) Snapshot of the rough crystalline (bottom) surface, taken at t=600 ps. Atoms are colored according to their z-coordinate. c) Linear dimension of the crystal growth front ($L_{cr}(t) - L_{cr}(t_0)$, see main text) as a function of time. The blue region mark the time lags in which the crystal growth proceeds in a linear fashion.

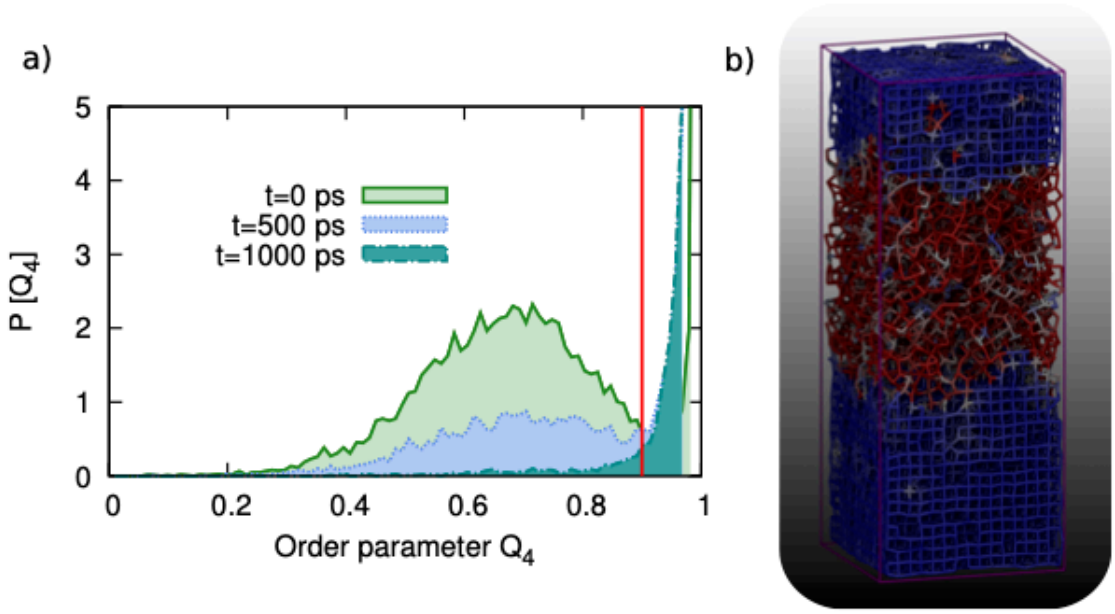

Fig. S6: a) Probability density distribution of the order parameter $\bar{Q}_4$ for M2 at 700 at t=0, 200 and 400 ps. The vertical line marks the threshold above which we consider an atom as crystalline. b) Snapshot of M2 at 700 taken after 200 ps. Each atom is colored according to the value of the order parameter.

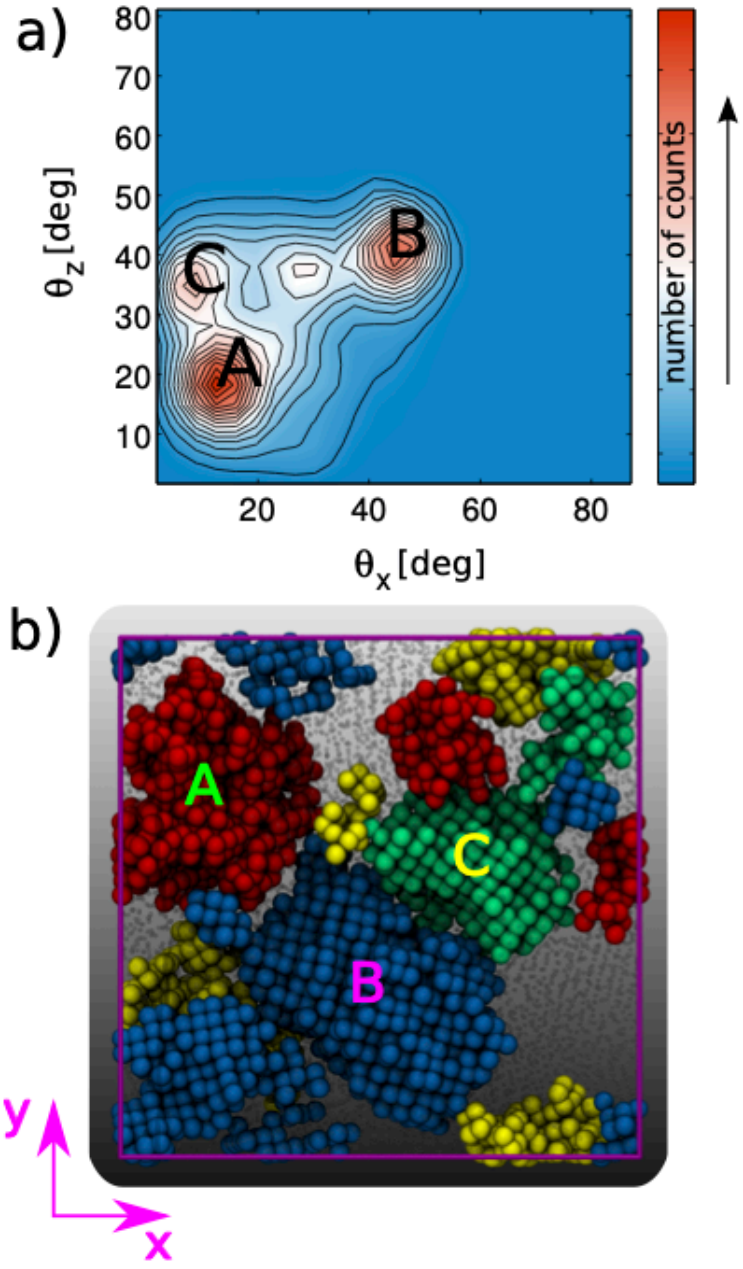

Fig. S7: a) Bi-dimensional projection of the $h(\theta_x, \theta_y, \theta_z)$ three dimensional histogram on the θ_x, θ_z plane. The three main angular domains are labeled alphabetically. b) Snapshot of the MP model at 700 K at the beginning of the simulation. The three biggest clusters are labeled according to panel a). Clusters A and B correspond to C_{111} and C_{100} grains in the main text.

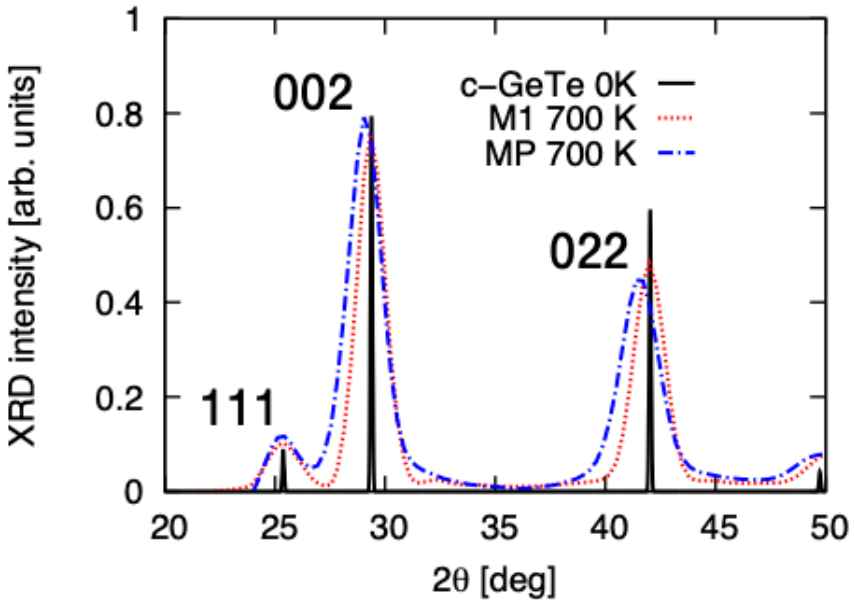

Fig. S8: XRD pattern of cubic GeTe at 0 K, and of the fully crystallized M1 and MP models at 700 K. The intensities have been renormalized so that the highest peak of each XRD pattern is equal to the arbitrary value of 0.8.

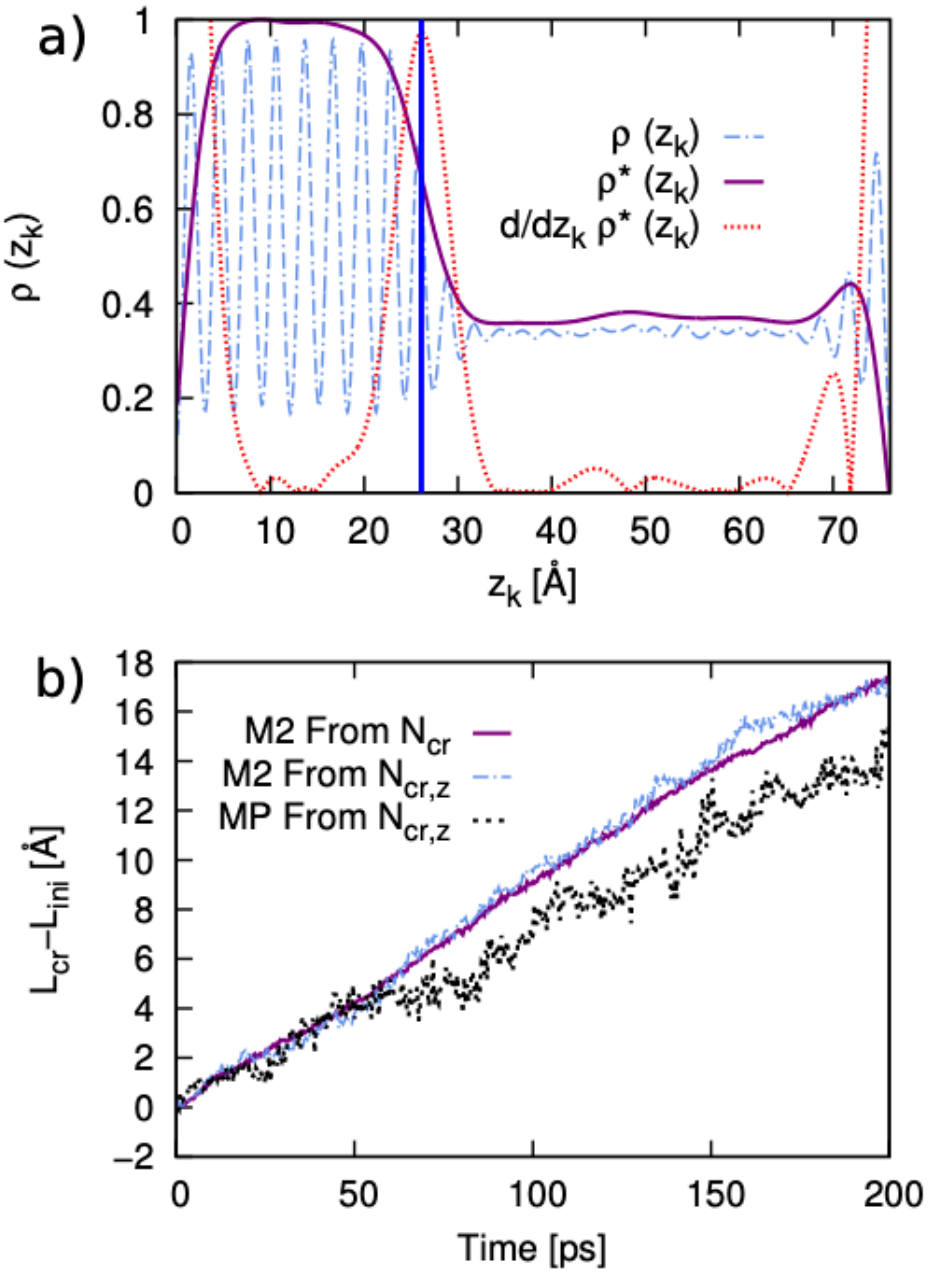

Fig. S9: a) Density profile weighted by the order parameter, $\rho(z_k)$, calculated along the z axis. In the same panel we report the filtered profile $\rho^*(z_k)$ (see text) and its derivative $d\rho^*(z_k)/dz_k$. b) Linear dimension of the crystalline phase as a function of time with respect to by its value at t=0. Results for M2 at 700 K are reported as obtained both from Eq. (3) in the main text (N_{cr}) and by the monitoring of the crystal growth front described here in the SI ($N_{cr,z}$). Results for MP are reported using the latter approach only.

References

(1) Smith, W. & Forester, T.R. DL_POLY_2.0: A general-purpose Parallel Molecular Dynamics Simulation Package. *J. Mol. Graph.* **1996**, *14*, 136-141.

(2) RuNNer. A Neural Network Code for High-Dimensional Potential-Energy Surfaces, Jörg Behler, Lehrstuhl für Theoretische Chemie, Ruhr-Universität Bochum, Germany.

(3) Bussi, G., Donadio, D. & Parrinello, M. Canonical Sampling through Velocity Rescaling. *J. Chem. Phys.* **2007**, *126*, 014101.

(4) Glazov, V.M. & Shelichov, O.D. Thermal-espansion and Characteristics of the Atomic Vibrations in Melts of IV-VI Compounds. *Sov. Phys. Semicond.* **1984**, *18*, 411-413.

(5) Sosso, G.C., Behler, J. & Bernasconi, M. (2012) Breakdown of Stokes-Einstein Relation in the Supercooled Liquid State of Phase Change Materials. *Physica Status Solidi B* **2013**, *249*, 1880-1885; erratum *250*, 1453.

(6) Sosso, G.C., Miceli, G., Caravati, S., Giberti, F., Behler, J. & Bernasconi, M. Fast Crystallization of the Phase Change Compound GeTe by Large-Scale Molecular Dynamics Simulations. *J. Phys. Chem. Lett.* **2013**, *4*, 4241-4246.

(7) Lechner W. Dellago C. Accurate Determination of Crystal Structures based on Averaged Local Bond Order Parameters *J. Chem. Phys.* **2008**, *129*, 114707-5

(8) Krbal, M.; Kolobov, A.V.; Fons, P.; Tominaga, J; Elliott, S.R.; Hegedus, J.; Giussani, A.; Perumal, K.; Calarcl, R.; Matsunaga, T.; Yamada, N.; Nitta, K.; Uruga, T.; Crystalline GeTe-based Phase-change Alloys: Disorder in Order. *Phys. Rev. B* **2012**, *86*, 045212-6.

(9) Hayward, J.A. & Haymet, A.D.J. The ice/water Interface: Molecular Dynamics Simulations of the Basal, Prism, $\{20\bar{2}1\}$, and $\{2\bar{1}\bar{1}0\}$ Interfaces of Ice Ih. *J. Chem. Phys.* **2001**, *114*, 3713-3726.